Sedimentary Geology 454 (2023) 106448

Contents lists available at ScienceDirect

Sedimentary Geology

journal homepage: www.elsevier.com/locate/sedgeo

Upper-flow regime bedforms in a subglacial triangular-shaped landform (murtoo), Late Pleistocene, SW Finland: Implications for flow dynamics and sediment transport in (semi-)distributed subglacial meltwater drainage systems

J. Hovikoski [a,*], J. Mäkinen [b], J. Winsemann [c], S. Soini [b], K. Kajuutti [b], A. Hepburn [d], A.E.K. Ojala [b]

[a] Geological Survey of Finland, Vuorimiehentie 5, FI-02151 Espoo, Finland
[b] Department of Geography and Geology, University of Turku, FI-20014, Finland
[c] Institute of Geology, Leibniz University Hannover, Callinstrasse 30, D-30167 Hannover, Germany
[d] European Space Astronomy Centre, European Space Agency, E-28692 Madrid, Spain

ARTICLE INFO

Article history:
Received 15 March 2023
Received in revised form 31 May 2023
Accepted 1 June 2023
Available online 8 June 2023

Editor: Dr. Brian Jones

Keywords:
Upper flow regime
Lower flow regime
Antidune
Humpback dune
Cyclic step
Chutes-and-pools
Murtoo
Subglacial
Meltwater route

ABSTRACT

We know less about subglacial meltwater flow properties in distributed inefficient and semi-efficient systems in comparison to those of ice marginal eskers and proglacial environments. While previous studies have indicated the overall common presence of upper-flow-regime (UFR) bedforms in glacigenic settings, facies expressions of subglacial meltwater flows remain poorly documented. Three ca. 3 m deep and up to 70 m long trenches excavated across a triangle-shaped subglacial landform called a murtoo in a Lateglacial to Holocene meltwater route in SW Finland provide a detailed window into sedimentary structures presumably formed ca. 40–50 km away from the coeval subaqueous margin of the Fennoscandian Ice Sheet (FIS). The aim of this paper is to document small-scale bedforms, which formed subglacially by meltwater flow and to characterize the proximal and central parts of the studied murtoo during its early evolutionary phase. We defined seven main facies types that characterize the depositional processes of the unit. Overall, the studied deposits reflect increasing meltwater delivery through time and are characterized by abrupt lateral changes in sedimentary structures and grain size. While the initial deposits are dominated by massive and horizontally laminated silt with sand lenses interpreted as lower-flow-regime deposits, the latter sediments are characterized by sinusoidal stratification, sigmoidal cross-stratification and scours with backsets or chaotic fill interpreted as deposits of antidunes, humpback dunes, chutes-and-pools and cyclic steps of the upper-flow regime. The upper-flow-regime bedforms developed on a 1 m high and 15 m long bed slope and are associated with the formation of a short-lived enlarged water-filled cavity or pond, where supercritical density flows allowed for the deposition of upper-flow regime bedforms. The final coarse-grained murtoo head-bar development, characterized by planar-cross stratified gravel and pebbly sand, indicates avalanche processes that were controlled by grain size.

Our results confirm that the core of the murtoo is depositional and meltwater processes played a key role in its deposition. Despite the subglacial setting with a subaqueous ice-sheet margin, the meltwater flow was not permanently characterized by pipe-flow conditions. Overall, the findings contribute to the understanding of semi-distributed subglacial meltwater systems during the retreat of a continental ice sheet (FIS) in a rapidly warming climate.

1. Introduction

Subglacial drainage systems form an important component in understanding glacier motion during climate warming (e.g., Schoof, 2010; Werder et al., 2013; Andrews et al., 2014; Nienow et al., 2017; Hart et al., 2022; Ravier et al., 2022; Simkins et al., 2023). In comparison to ice-marginal tunnel channels/valleys and eskers, the nature of subglacial meltwater routes remains poorly understood. As subglacial environments are difficult to monitor directly, glacial landforms and their sedimentary structures can provide critical information about the past glacial hydrology and help to characterize the spatial and temporal evolution of subglacial drainage systems (Hooke, 2019).

* Corresponding author.
E-mail address: jussi.hovikoski@gtk.fi (J. Hovikoski).

https://doi.org/10.1016/j.sedgeo.2023.106448

Recent advances in LiDAR-based (light detection and ranging) landform mapping have shed light on the dynamics of glacier meltwater routes during the Weichselian deglaciation, extending tens of kilometers below the Fennoscandian Ice Sheet (FIS) (e.g., Mäkinen et al., 2017; Peterson and Johnson, 2017; Dewald et al., 2022; Ahokangas et al., 2021; Peterson Becher and Johnson, 2021; Ojala et al., 2022). Lately, a distinct triangle or V-shaped subglacial landform called 'murtoo' was described in the FIS area in Finland and Sweden (Mäkinen et al., 2017; Ojala et al., 2019; Peterson Becher and Johnson, 2021). These landforms were formed in areas with excessive meltwater delivery to the bed during warming climate and rapid retreat of the continental ice sheet. Murtoos generally occur in clusters and along meltwater corridors, pointing out an important role of subglacial hydrology in their formation (Ojala, 2019). Based on their spatial distribution in the FIS area, morphometric relationship with meltwater corridors, eskers, and ribbed moraines, as well as internal sediment characteristics, it has been proposed that murtoos represent a transitional form between inefficient non-channelized (distributed) and efficient channelized (esker tunnels) subglacial drainage systems (e.g., Ojala, et al. 2019, 2021, 2022; Peterson Becher and Johnson, 2021).

According to the current understanding, murtoos are subglacially formed depositional landforms with erosional sides and triangular heads. Previous observations have suggested that murtoos and murtoo-related landforms can be diverse including triangle-type, chevron-type and lobate-type murtoos, which are often associated with ridges and escarpments (Ojala et al., 2021). They consist of sorted and stratified sandy sediments and coarser diamictic material (Peterson Becher and Johnson, 2021; Ojala et al., 2022). The hypothesis is that murtoos are depositional landforms with erosional sides and heads, initially formed in a network of low canals and conduits or cavities with fluctuating stream flow likely over 50 km from the ice margin (Mäkinen et al., 2019, 2023). Their sediments exhibit an increasing influence from repeated influxes of glacier meltwater distributed in widening broad and low conduits with increasing sediment transport over short distances, thus suggesting shifting toward semi-distributed drainage (Mäkinen et al., 2019, 2023; Ojala et al., 2022). However, their internal structures and genesis remain inconclusively documented and understood. In general, glacigenic environments are typified by temporally powerful meltwater discharge, which varies on short time scales (from hours to seasons, e.g., Shepherd et al., 2009; Bartholomew et al. 2010). The strong discharge, especially when associated with shallow water depth, favors the development of near critical to supercritical flow conditions, where the Froude number (a ratio of inertial to gravitational forces) approaches or exceeds unity (e.g., Allen, 1982; Lang et al., 2021a, 2021b). When coupled with high sediment supply, upper-flow-regime (UFR) bedforms—e.g., upper-stage-plane beds, antidunes, chutes-and-pools and cyclic steps—may be preserved. Upper-stage-plane beds are expressed by horizontally stratified sand, which consists of low amplitude bed waves or sheets (Paola et al., 1989; Best and Bridge, 1992). Such beds can gradationally overlie sigmoidal cross-stratification (deposited by humpback dunes or downslope migrating antidunes), recording the transition between dunes and upper-stage-plane beds or stable antidunes (e.g., Saunderson and Lockett, 1983; Fielding, 2006; Lang and Winsemann, 2013). Stable antidunes have an in-phase relationship with the upper boundary of the flow until the wave steepens and starts breaking (e.g., Kennedy, 1963; Hand, 1974; Allen, 1982; Alexander et al., 2001; Spinewine et al., 2009; Cartigny et al., 2014). Depending on grain-size and Froude number they may be either stationary or migrate upslope or downslope. The resulting sedimentary structures may consist of sinusoidal stratification, low-angle cross-stratification or shallow scour-fills with backsets. Chutes-and-pools and cyclic steps develop under higher Froude numbers and are characterized by unstable flows with alternating supercritical and subcritical flow stages separated by hydraulic jumps (see Slootman and Cartigny, 2020 and Slootman et al., 2021 for reviews). While cyclic steps form trains of bedforms with a constant distance, chutes-and-pools appear to be more transient features with erratically occurring hydraulic jumps (Lang et al., 2021b; Slootman et al., 2021).

Previous work has demonstrated that UFR-bedforms are common in glacial environments both in subaqueous and subaerial settings including proglacial environments (Hirst et al., 2002; Russell et al., 2003, 2007; Winsemann et al., 2009, 2018; Girard et al., 2012; Lang and Winsemann, 2013; Dietrich et al., 2016; Lang et al., 2017b; Ghienne et al., 2021) as well as subglacial eskers and tunnel channels/valleys occurring near the ice-sheet margin (Brennand, 1994; Burke et al., 2008, 2010; Fiore et al., 2002; Lee et al., 2015; see Lang et al., 2021b for review). In contrast, subglacial drainage systems and their sediments, developing tens of kilometers away from the ice-sheet margin, are only poorly documented (e.g., Simkins et al., 2023). In case of fully water filled cavities or conduits, pipe-flow conditions may occur suppressing the development of most UFR bedforms (Banerjee and McDonald, 1975; Cartigny et al., 2014; Lang et al., 2021b). However, density flows may develop in subglacial ponds or lakes (e.g., McCabe and ÓCofaigh, 1994; Munro-Stasiuk, 2003; Hodgson et al., 2009; Remmert et al., 2022), leading to the deposition of supercritical bedforms (cf. Fedele et al., 2016; Lang et al., 2021a, 2021b; Winsemann et al., 2021).

The meltwater flow properties and its spatial and temporal evolution in subglacial semi-efficient drainage systems are controlled by different parameters (e.g., Simkins et al., 2023). Most notably, the meltwater flow in subglacial semi-efficient drainage systems is strongly affected by the pressure generated by the weight of the overlying ice, influencing water flow orientation and its velocity. Moreover, the shallow space forming below the ice and bed/bedrock is continuously evolving, being controlled by short-lived and seasonal changes in meltwater discharge and resulting changes in drainage efficiency and effective pressure (Lesemann et al., 2010). Drop in the water pressure leads to creep closure and ice–bed coupling complicating the formation of permanent channels (e.g., Schoof, 2010). Another important challenge is glacial erosion and deformation, which may inhibit preservation of the original sedimentary structures in subglacial settings. Earlier sedimentological studies on murtoos in Finland have concentrated on the distal parts characterized by boulders (Mäkinen et al., 2023). Peterson Becher and Johnson (2021) report sorted sandy and silty sediments from murtoo interiors in southern Sweden, but these sediments do not show clear sedimentary structures deposited by meltwater and are more heavily deformed by ice.

Here, we report well-preserved sediments deposited by subglacial meltwater flow from a triangle-type murtoo (Ojala et al., 2021) along a Lateglacial to Holocene subglacial meltwater route in SW Finland, deposited presumably 40–50 km (Ojala et al., 2019) away from the coeval subaqueous ice-sheet margin. While Ojala et al. (2021) and Mäkinen et al. (2023) excavated murtoos perpendicular to their long-axes and close to the triangular tip of the murtoo, the present excavation was conducted longitudinally through the entire murtoo from its proximal to distal side, supplemented with proximal and distal trenches perpendicular to the long-axis of the murtoo (Fig. 1). The purpose of the paper is twofold: i) to contribute to the understanding of the genesis and early evolutionary development of the murtoo landform and the transition from inefficient toward efficient meltwater delivery systems and ii) to document the diversity of small-scale subcritical and supercritical bedforms deposited by the meltwater in shallow (semi-)distributed subglacial meltwater drainage systems.

2. Study area and methodological approach

Our study site lies within the area covered by the Baltic Sea Ice Lobe of the FIS during the Late-Weichselian to Holocene deglaciation (Palmu et al., 2021; Stroeven et al., 2016) (Fig. 1). The area was deglaciated between 10.8 and 10.9 cal ka BP (Stroeven et al., 2016) and is characterized by several subglacial meltwater corridors (Ahokangas et al.,

Fig. 1. A) The location of the studied triangle-type murtoo along a subglacial meltwater route in the Lake Sääksjärvi vicinity in SW Finland. B) Distribution of triangle-type murtoos in Sweden (Ojala et al., 2019), all types of murtoos (Ojala et al., 2021) in Finland, and the main ice-flow patterns (black lines) and the ice-marginal formations (green lines) in Finland (Boulton et al., 2001). C) The studied murtoo in Myllykoski is orientated along ice-flow direction and has a relief of 2–3 m above the surrounding area. The hill-shaded digital elevation model is based on onsite measurements of LiDAR with 0.1 m resolution.

2021) in association with the Lake Sääksjärvi. Murtoo fields in the area are associated with these meltwater routes, along with an abundance of hummocky moraine fields. The proglacial water depth reached approximately 100 m during the time of deposition (Ojala et al., 2013). The presently studied triangle-type murtoo is ca. 40 m wide, 80 m long and has a relief of about 2 m (Figs. 1C, 2). As a common feature for the triangle-type murtoos, the longitudinal profile is asymmetric with a shorter and steeper distal slope compared to the longer and gentler proximal slope (Ojala et al., 2019) (Fig. 1C). The sides of the murtoo are straight and steep, and a tip of the murtoo is oriented parallel to the ice-flow and meltwater route direction (Fig. 1A). The proximal side at the western end of the murtoo comprises a shallow fan-shaped hollow, which may represent a subglacial erosional area that is related to the murtoo forming process (see Mäkinen et al., 2017, 2023).

Prior to excavations, the triangle-type murtoo was scanned with a terrestrial LiDAR system and studied with a GSSI SIR-3000 ground penetrating radar (GPR) using a 200 MHz antenna. The murtoo sediments were investigated by trenching 2–4 m wide and up to 3 m deep sections perpendicular and longitudinal to the landform (Fig. 1C). The position and elevation profiles of these trenches were measured with real-time-kinematic (RTK) GPS. The trench bottom was excavated deeper in 3 test pits, reaching the underlying till and groundwater table (Figs. 2A, 3). The till bed and the bedrock level along the trenches were interpreted from the GPR profiles.

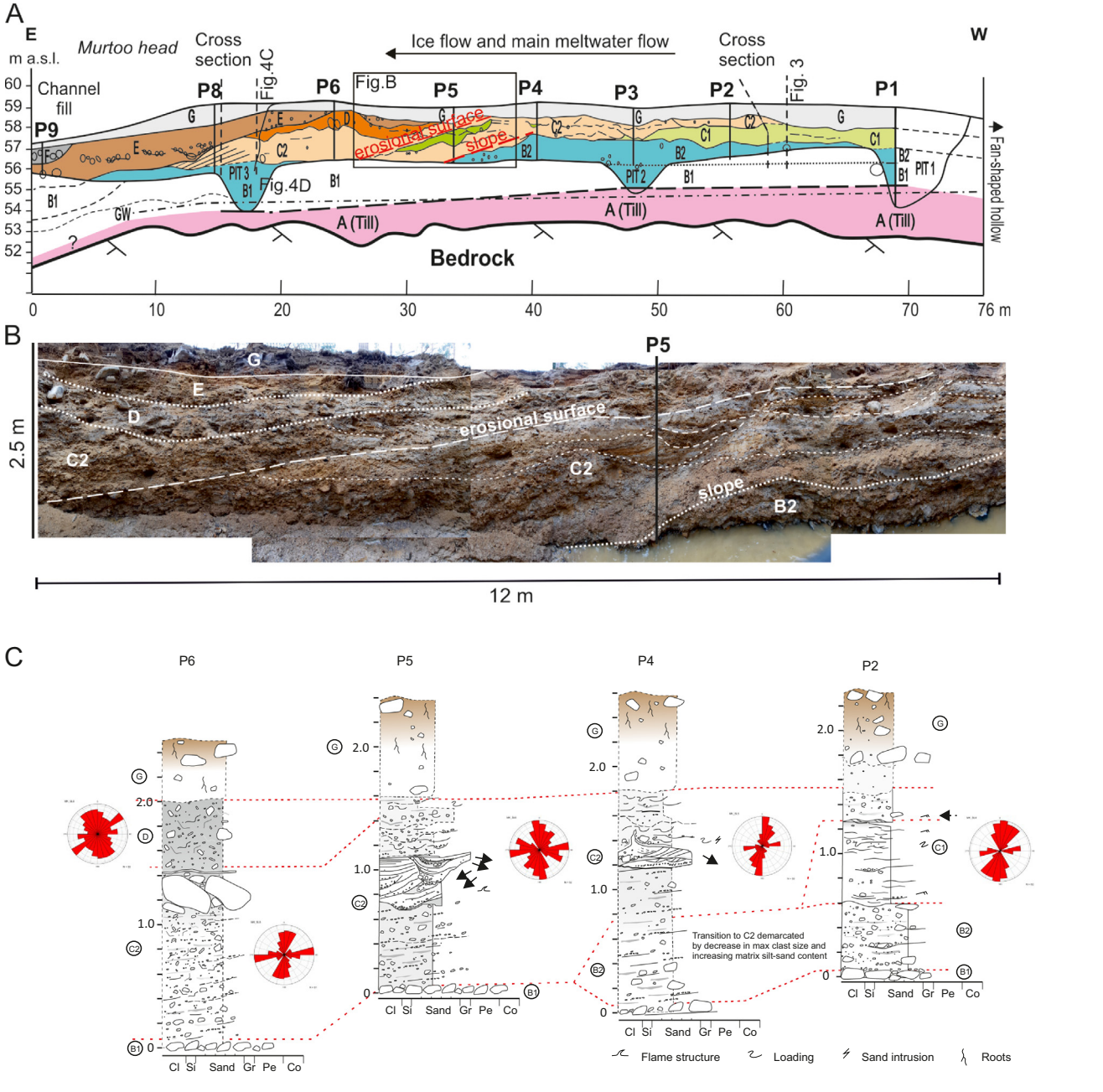

Fig. 2. A) Distal–proximal cross-section of the studied murtoo illustrating stratigraphic units (A–G) and locations of the sedimentological logs. This study concentrates on Unit C that contains Sub-units C1 (silt dominated) and C2 (sand-dominated). B) A photo-panorama illustrating characteristics of Sub-unit 2. Note the bed-slope with apparent eastward dipping orientation. See Figs. 7 and 8 for facies details. C) Selected sedimentological logs covering the studied interval. Clast measurements (rose diagrams) and paleocurrent measurements from cross-stratification (arrows) are shown. Note that the present profile is drawn from the southern wall of the excavated trench, thereby pointing to the opposite direction than presented in the index map (Fig. 1).

Documentation of the excavated exposures was done by photo mosaics and logging of sections to reconstruct the sedimentary facies and lateral facies relationships along the triangle-type murtoo system. Outcrop descriptions include data on bed dip, grain size, sorting, roundness, clast fabric, sedimentary structures and bed geometry. The fabric notation uses symbols a and b for the clast long and intermediate axes.

3. Results and interpretation

3.1. Depositional units of the studied murtoo

The studied murtoo can be divided into 7 main depositional units (Units A–G; Figs. 2A–C, 3, 4A–D). Below, each unit is first briefly summarized. The main focus of the study, Unit C, is subsequently described and interpreted in more detail.

The lowermost Unit A comprises a regionally continuous, bluish silty till bed that rests on bedrock. The unit is sharply overlain by Unit B that forms a continuous, horizontal base of the murtoo and is generally poorly exposed but can be divided into two subunits (B1 and B2). Based on GPR profiles and test pits, the unit is 1.0–2.5 m thick (Fig. 3). Subunit B1 consists of poorly sorted and crudely horizontally stratified, bouldery gravel (Fig. 4A) pointing to winnowing by flowing water and lag formation.

The lowermost gravel on top of the silty till is silty and wet, and the largest clasts are subrounded to rounded (Fig. 4D). The largest boulders are bladed and horizontally orientated. The c-axis is ca. 0.5 m long,

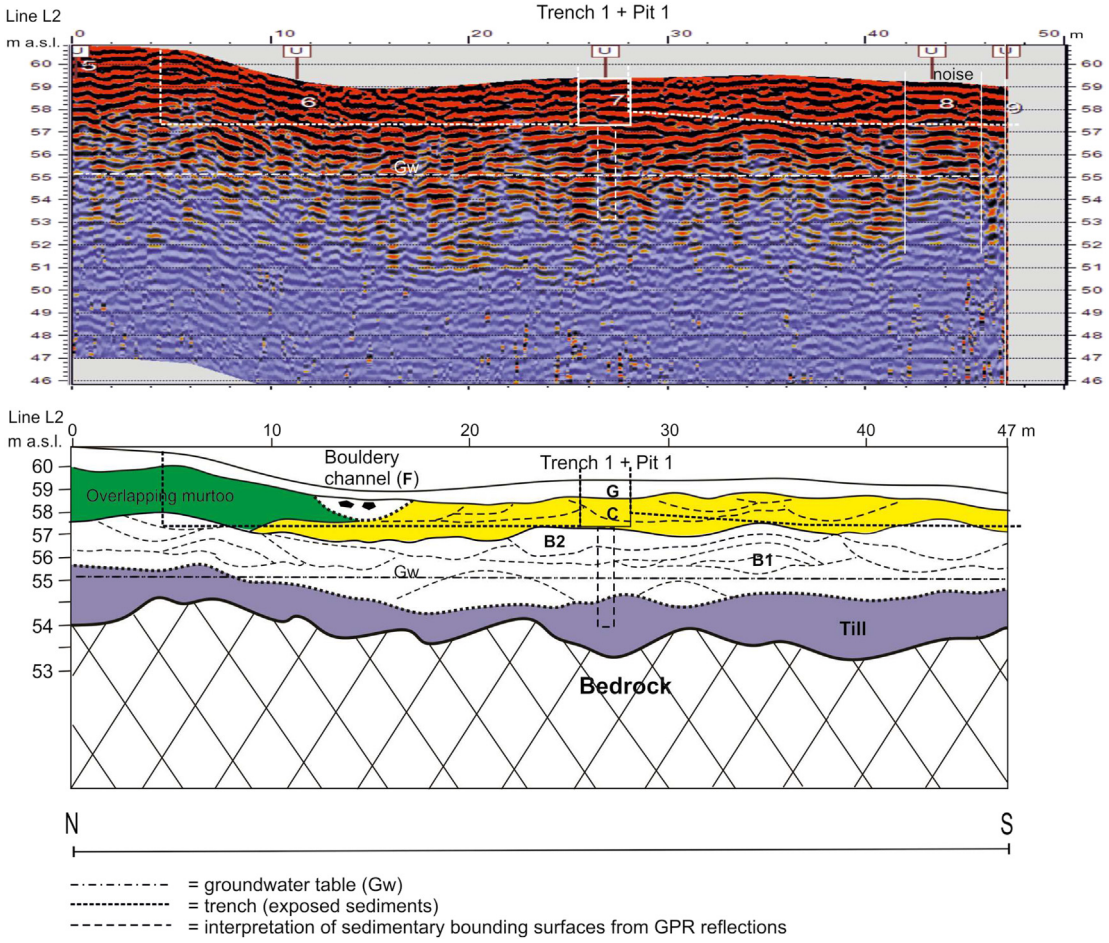

Fig. 3. Proximal cross-section of the murtoo. The cross-section is based on GPR with 200 MHz antenna (0.15 m resolution) and reference data from trench 1 and Pit 3. Unit B represents the meltwater route deposits and Unit C the murtoo sediments studied herein. A bouldery channel fill with clay (Unit F) separates the studied murtoo from the overlapping, neighboring murtoo. The depth scale of the GPR profile is corrected below the groundwater table.

whereas the a-axis length can exceed 1.0 m. Horizontally oriented boulders often show well-polished upper surfaces suggesting contact with overlying ice and abrasion. The cross-section across the head of the murtoo reveals a locally arched architecture with crude stratification of the largest clasts (Fig. 4A). Arched architecture (1–2 m high and 4–10 m wide) is also a common feature outlined from the proximal GPR profile (Fig. 3).

Subunit B2 is characterized by upward fining, weakly stratified pebbly sand that contains laterally discontinuous lenses of clast-supported pebbles/cobbles and pebbly sand. Clasts are subangular to subrounded. The subunit also includes patches of structureless silt or silty fine sand. The stratification is characterized by crudely inclined beds with apparent dip toward the East (i.e., parallel to the murtoo axis toward the head of the murtoo) or weakly defined troughs revealed by cobble lags. The contact between subunits B1 and B2 is gradational and it is difficult to separate them from the GPR profiles. Unit B is interpreted to represent deposition along the wider meltwater route with development toward a semi-distributed drainage system represented by the overlying murtoo.

Unit C sharply overlies Unit B and forms the main body of the murtoo. It can be subdivided into Sub-units C1 and C2 (Fig. 2). Subunit C1 is dominated by silt and sand, 0.6–1.0 m-thick and ~45 m long, forming most of the sediment volume in the proximal part of the murtoo (Fig. 5A–C). It continues laterally along the whole proximal cross-section until it becomes eroded by marginal channels (Unit F) of the murtoo. Upward and toward the distal tip, Sub-unit C1 is replaced by sand dominated Sub-unit C2. Around profiles P4 and P5 (Fig. 2A, B), an eastward dipping bed slope occurs. The slope has a relief of ~1 m and continues laterally for ~15 m. Sub-unit C2 terminates near the murtoo tip, where it consists of inclined gravelly sand beds that onlap a trough-shaped depression several meters wide on the top of the underlying unit B2 (Fig. 4A, C). Moreover, in its distal end, Unit C2 is overlain by a laterally restricted occurrence of compacted diamicton (Unit D; Figs. 2A, 4C). This diamicton represents the final sedimentation in the proximal half of the central murtoo. The subsequent, channelized meltwater flow bypassed the central zone along the northern and (to minor degree) southern margins of the murtoo and is characterized by erosionally-based upward-fining successions consisting of boulders, gravel and sand (Unit E; Fig. 4A, B). Muddy, clay-rich sediments represent the final deposition in the marginal channels (Unit F) and represent the abandonment and the end of murtoo sedimentation. The murtoo is mantled by a loose, 0.5–1.0 m-thick, bouldery diamicton (Unit G) that has been altered by later shoreline processes, bioturbation, podsol soil development and frost-heave. This study focuses on the lateral and vertical facies relationships of Unit C that form the main body of the murtoo (Fig. 2A–C).

3.1.1. Facies of Unit C

Unit C is composed of 7 facies types (F1–F7) described and interpreted in Table 1 and illustrated in Figs. 5–8. Generally, Unit C is silt-dominated in the proximal part (Sub-unit C1) and gets sandier toward the distal end (Sub-unit C2). Laterally, toward the sides of the murtoo, Unit C shows slump-folding and other syn-sedimentary soft-sediment deformation that is restricted to specific beds.

Sub-unit C1 is characterized by decimeter-scale beds comprising interlaminated silt and very fine to fine grained sand, with local mm-

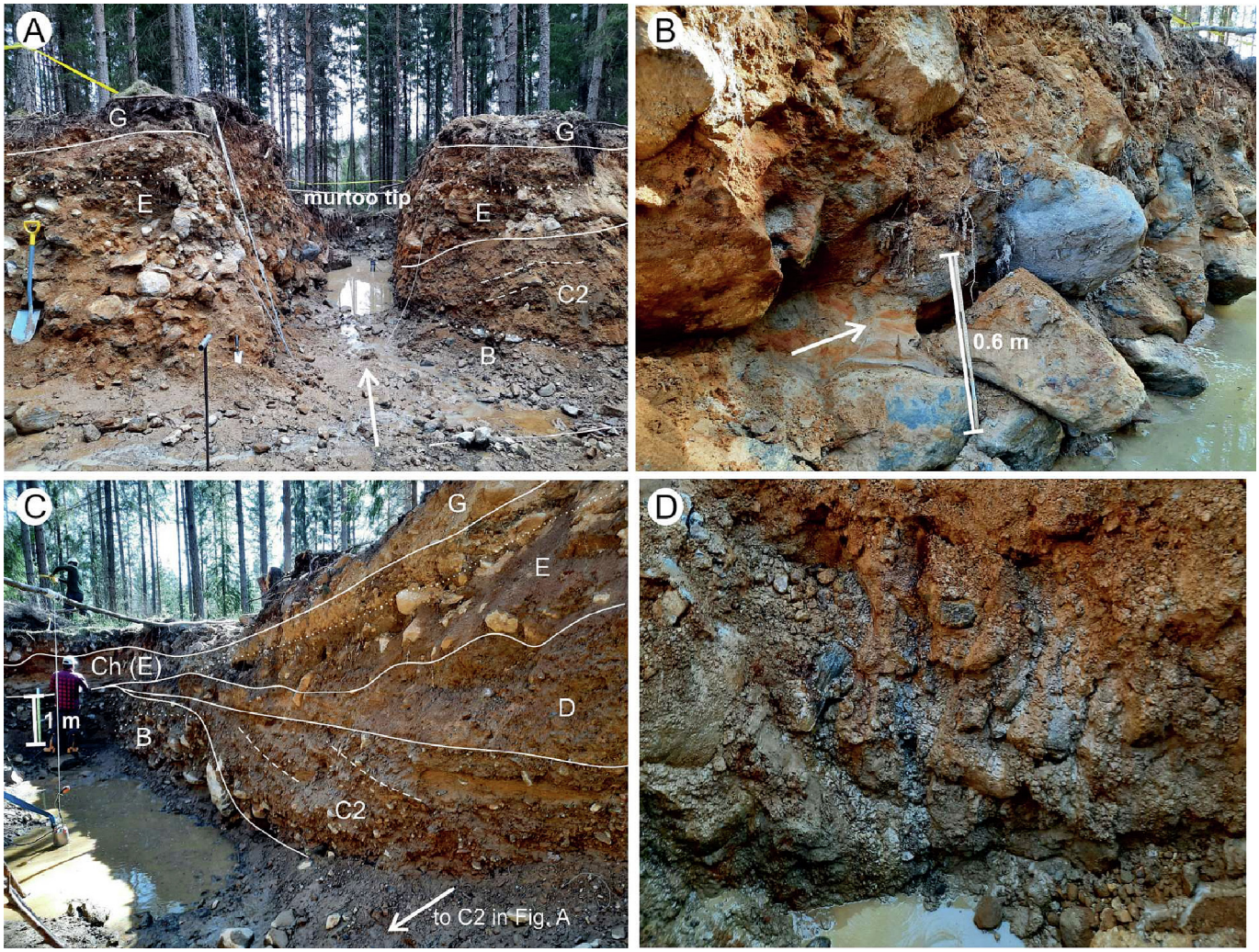

Fig. 4. Deposits from the distal head of the murtoo. A) View from the distal cross-section toward the murtoo tip. Note the head bar sediments (F7, Sub-unit C2) on top of the meltwater route deposits (Unit B), bouldery channel deposits (Unit E) and the topmost loose diamicton, covering the whole murtoo (Unit G). B) Closer image of bouldery channel fill deposits close to the murtoo tip. Flow direction is indicated with an arrow. C) Deposits in the southern part of the distal cross-section. Note the arched deposits of Unit B and lateral, stratified head bar deposits (Unit C2) overlain by diamicton (Unit D). Unit D was partly eroded by a channel along the murtoo margins (Unit E). The murtoo and its marginal channel fill are topped by a loose diamicton (Unit G). D) Poorly sorted gravel of Unit B with leaking groundwater in Pit 3 close to the tip of the murtoo. Unit B represents deposition within the meltwater route prior to murtoo formation. Note the lack of clayey, fine-grained matrix and roundness of the clasts.

scale sand lenses (F1) (Fig. 5A). In addition, structureless-appearing up to 5 cm thick silt beds with pebbles derived from the ice-roof (F1) as well as lenticular beds of sandy gravel (F6) are locally present. The lenses are commonly 30–50 cm wide and ~10 cm thick. Finally, subordinate facies include ripple-scale climbing bedforms with apparent westward (upstream) climbing direction (F2) and sinusoidally stratified medium-grained sand (F3) (Fig. 5A–D; Table 1). The clast fabric shows dominance of transverse clast orientation (a-axis N–S oriented, Fig. 2C).

Sub-unit C2 comprises silt-laminae and interbeds (F1), ripple-scale symmetrical or climbing bedforms (F2), sinusoidally stratified sand (F3), scours with structureless or backset-cross-stratified pebbly sand (F5), sigmoidal cross-stratification (F4), and trough and planar cross-stratification (F7) (Figs. 6–8; see below). The large-scale (~80 cm high and several meters wide) cross-stratification shows E–NE oriented cross-strata in the distal end, whereas the sigmoidal cross-stratification is oriented toward the E–ESE, following broadly the eastward dipping bed slope as well as the general orientation both of the meltwater route and the murtoo landform (Fig. 1A and C). Upcurrent (W–SW) oriented cross-stratification occurs in scour fills or as small-scale climbing bedforms (see below). Clast fabric measurements show common transverse clast orientation (a-axis N–S oriented), but with increasing scatter and flow parallel clast orientation (Fig. 2C).

On the bed slope, the deposits become typified by abrupt lateral changes in sedimentary structures and grain size associated with cm- to dm-scale changes in bottom topography (Fig. 2B). The irregular topography is primarily formed by lateral trains of erosional scours separated by convex surfaces. The individual facies commonly form compound bedforms and facies transitions; these occurrences are summarized below.

3.1.2. Lateral and vertical associations of sigmoidal cross-stratification (F4) and sinusoidal to subhorizontal stratification (F3)

Down-current (E–SE) migrating sigmoidally cross-stratified fine to very coarse-grained sand (F4) occurs on an eastward-dipping bed slope, either overlying a flat surface with a sandy silt drape on the upper portion of the slope or a scour fill (20 cm wide and 60 cm deep) near the base of the slope (Figs. 6A, B and 7A, B, C). The deposits commonly display differentiation into topset, foreset and bottomset laminae. Topset laminae are subhorizontal to sinusoidal and the contact between foreset and topset laminae may be erosional or transitional. Vertically stacked cross-sets are developed on the upper portion of the slope, which are separated by an erosional surface. The lower foreset deposits downlap onto the basal surface and display a transition between convex foreset beds and subhorizontal topset beds with rising and

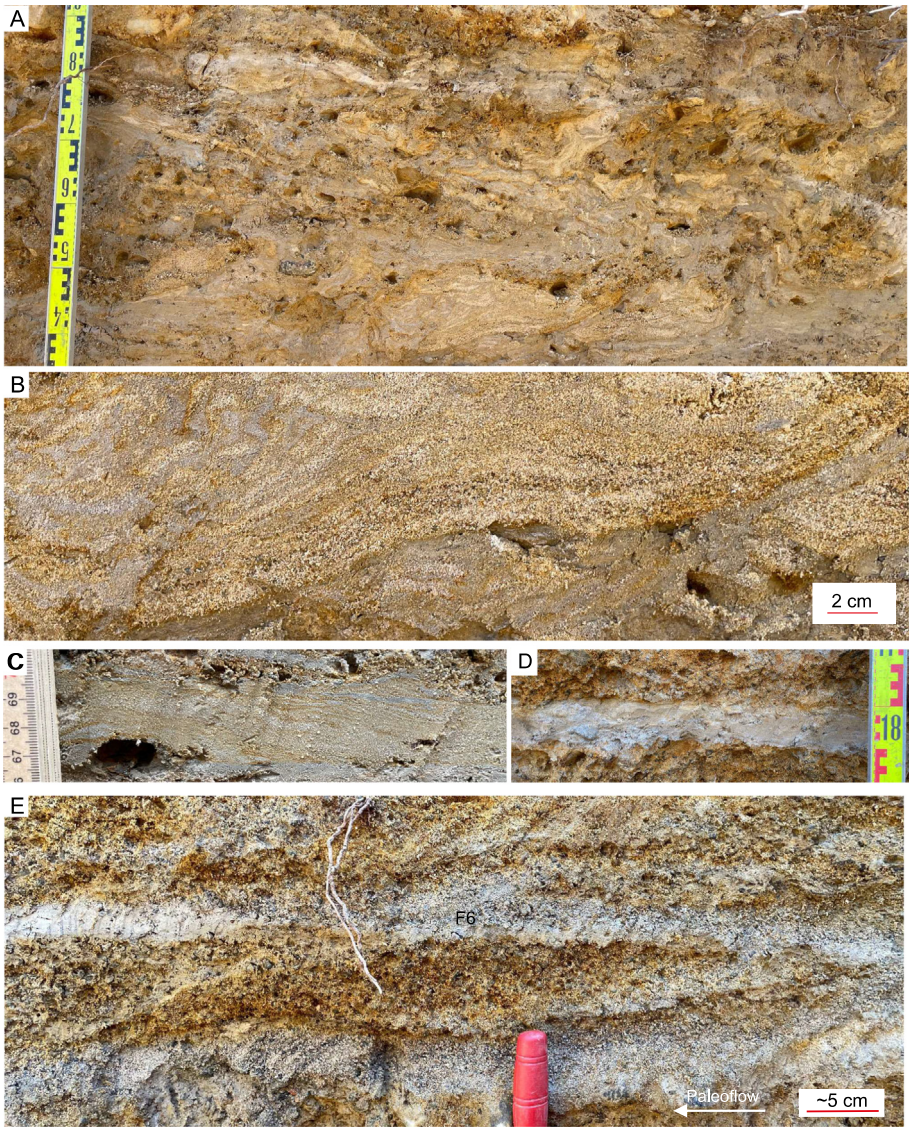

Fig. 5. Facies examples of Sub-unit C1. A) Deformed silt–sand heteroliths showing loading and slumping toward the northern lateral margin of the murtoo (F1). View toward the West. B) Example of sinusoidal stratification overlain by deformed silt–sand couplets. C) Ripple-scale climbing bedforms with apparent upstream oriented (West) climbing orientation. View toward the south. D) Structureless mud bed with pebbels . View toward the south. E) Lenticular sandy gravel. View toward the south.

falling brink trajectories (Fig. 6B). This sigmoidal cross-set is erosively overlain by smaller-scale straight foreset beds, which in turn are erosively overlain by sinusoidal topset beds. Downstream, the sigmoidally cross-stratified deposits are overlain by deformed thin-bedded (0.5–1 cm) sand-mud couplets and structureless sand (Fig. 6A, B).

On the lower portion of the slope, sigmoidally cross-stratified medium- to very coarse-grained sand infills a scour and overlies deformed sediments showing structureless sand and flame structures (Fig. 7A, B). The foreset deposits downlap onto the basal scour surface and display a transition between concave foreset beds and subhorizontal topset beds with a subhorizontal brink trajectory (Fig. 7B). In down-flow direction, the sigmoidally cross-stratified sand passes into sub-horizontally stratified medium-grained sand (Fig. 7C). Upstream, the sigmoidally cross-stratified sand is erosively overlain by a scour fill with backsets (Fig. 7A).

3.1.2.1. Interpretation. Sigmoidal cross-stratification commonly forms under transcritical and/or supercritical flow conditions, either representing deposits of humpback dunes or downstream migrating antidunes (Fielding, 2006; Lang and Winsemann, 2013; Fedele et al., 2016; de Cala et al., 2020; Lang et al., 2021b) or progradational infills of scours (Lang and Winsemann, 2013). The different topset–foreset contacts and trajectories of topset–foreset transitions point to different rates of deposition. Rising or horizontal brink trajectories indicate the highest rates of deposition, whereas falling brink trajectories are commonly related to the filling of troughs (e.g., Lang and Winsemann, 2013). The vertical and lateral transition from humpback-dune geometries into sinusoidal or subhorizontal geometries indicates the formation of antidunes or upper-stage plane beds, caused by flow thinning and acceleration above the humpback dune. Erosive topset–foreset contacts commonly are related to low sediment supply. The formation of scours and deposition of deformed strata in the lee of the humpback dunes may be related to the formation of local hydraulic jumps and slumping (e.g., Lang and Winsemann, 2013).

3.1.3. Lateral and vertical associations of scour fills (F5) and sinusoidal stratification (F3)

Scours with massive or deformed chaotic infill or with up-current oriented cross-stratification (F5) are common in various portions of the bed slope. The scours are typically 30–50 cm wide and 10–25 cm deep. They occur either as isolated features or are laterally offset

Table 1
Main facies types characterizing the proximal half of the studied murtoo (Sub-units C1 and C2).

Facies	Description	Interpretation	Figures
F1: Massive and horizontally laminated silt with sand lenses	Silt-laminae or structureless-appearing silt beds. Laminae are from sub-mm to 2 mm thick, and alternate with typically mm-scale sand lenses. The lenses show locally downstream oriented ripple cross-lamination. Silt beds are few cm-thick and commonly contain pebbles derived from the ice-roof. F1 shows commonly soft-sediment deformation.	Suspension settling and deposition by low-energy subcritical flows	5A, D
F2: Ripple-scale symmetrical or upstream climbing bedforms	Ripple-scale climbing bedforms in very fine to fine-grained sand. The angle of climb ranges between critical and supercritical. Bedforms are climbing upstream. The crests of symmetrical bedforms are offset. Wave-lengths range between ~3 and ~5 cm.	Deposition of small-scale antidunes and/or cyclic steps by supercritical flows. The upstream and downstream migration of non-breaking antidunes caused the slight upflow and downflow offset of wave crests. Some examples, which are not associated with F3, may represent backflow ripples.	5C, 8C
F3: Subhorizontally to sinusoidally stratified sand	Mostly medium-grained, sinusoidally or subhorizontally stratified sand. Contains locally coarse sand and granules. Beds are a few cm to 10 cm thick.	Deposition of stable antidunes or plane beds by supercritical flows	5B, 6B, 7B, C, 8B, C
F4: Sigmoidally cross-stratified sand	Fine to very coarse-grained, cross-stratified sand, with well-developed bottom sets. Subhorizontally to sigmoidally stratified topsets are locally developed. Cross-set height is 10–20 cm.	Deposition of humpback dunes or downslope migrating antidunes by transcritical to supercritical flows. Partly progradational infills of scours.	6B, 7B
F5: Scour fills with pebbly sand	Scours with a fill of structureless or chaotic pebbly sand or with upcurrent dipping stratification that comprise fine to medium grained sand or granules. The scours are 40–100 cm wide and 10–25 cm deep.	Rapid sedimentation following scour formation (hydraulic jump?), possibly representing deposits of chutes-and-pools or cyclic steps.	6C, 7A, B, D, 8A
F6: Lenticular sandy gravel	Poorly-sorted and mostly ungraded lenticular sandy gravel comprising typically sand, granules and pebbles. Gravel lag may occur at the base. The lenses are 5–30 cm thick and 20–150 cm long.	Infills of small and shallow channels. Braid bar deposits?	5E
F7: Trough and planar cross-stratified pebbly sand and gravel	Crudely-developed trough cross-stratified or planar cross-stratified pebbly, medium to coarse grained sand or sandy gravel, with dm-scale (~10–~80 cm) set thickness. Locally present are patches of structureless silty fine-grained sand.	Deposition by migrating 3D dunes from subcritical flows. Large planar cross-stratification represents a bar-like unit prograding downstream, forming the initial head of the murtoo.	4A, C

stacked. Where visible, the lateral spacing between two scours is ~1 m (Fig. 7D). Between the scours thin sinusoidally stratified sand beds occur (F3) with wavelengths of ~10–~20 cm (Fig. 8B, C). The sinusoidally stratified sand is partly overlain by symmetrical ripple-scale climbing bedforms (F2) with slightly up- and down-current oriented climbing patterns (Fig. 8C). The scour infills are ranging from structureless sand with outsized clasts (up to 10 cm in diameter), deformed thin-bedded sand-mud couplets, to up-current oriented (W–SW) cross-stratified sand and pebbly sand. Sandy cross-sets are ~5–~10 cm thick and cross-sets of pebbly sand ~10–~15 cm thick. (Figs. 7D, 8A). Commonly, the up-current part of scours is filled with deformed deposits with outsized clasts, whereas the down-current part is filled with structureless sand or up-current oriented stratification (Fig. 8A). The successive scour fills become younger upstream.

3.1.3.1. Interpretation. Laterally offset-stacked scours, filled with deformed sediments and backsets point to the deposition by upslope migrating cyclic steps, whereas isolated scour fills with backsets may represent chutes-and-pools (cf., Cartigny et al., 2014; Lang et al., 2017a, 2017b, 2021b; Winsemann et al., 2018; Slootman and Cartigny, 2020). The formation of dewatering structures in some scours indicates rapid suspension settling and pressure fluctuations in hydraulic-jump zones (Postma et al., 2014).

The lateral and vertical association with sinusoidal stratification and up-current aggrading climbing bedforms indicate deposition by stable antidunes that may have formed on the stoss side of cyclic steps during flow re-acceleration. Similar successions have been described by Lang et al. (2017a). The symmetrical ripple-scale bedforms with offset crests and/or upstream climbing patterns are interpreted as small-scale antidunes (Tan and Plink-Björklund, 2021). The upstream and downstream migration of non-breaking antidunes caused the slight upflow and downflow offset of wave crests (Lang and Winsemann, 2013; Lang et al., 2017a, 2017b, 2021b).

4. Discussion

4.1. Implications for subglacial meltwater routes and development of murtoo landforms

The results provide a rare insight into subglacial meltwater flow properties within a transition from a distributed/inefficient system to a semi-distributed/semi-efficient drainage system associated with enlarging cavities. In previous works in Finland, murtoos have been excavated in their elevated distal parts restricted to the triangular-shaped tip, whereas their lower proximal part has received less attention. Importantly, the results of this case study indicate that the core of the murtoo in the proximal part is depositional and that subglacial meltwater flows played a key role in its formation. Erosional processes have been found to be significant at later evolutionary phases of murtoo evolution (Mäkinen et al., 2017, 2023, Ojala et al., 2022, Peterson Becher and Johnson, 2021), which is the case also in the studied murtoo (Units E and F).

The stratigraphic evolution of the studied murtoo is interpreted and summarized as follows (Figs. 9, 10):

The murtoo developed on the boulder and gravel dominated Unit B (Phase 1 in Fig. 10). Its sedimentological characteristics such as sediment sorting, lag deposits and crude inclined stratification indicate that its deposition was influenced by flowing water above the underlying silty till. The alignment of the largest clasts and their polished upper surfaces proposes that the height of the depositional space (<0.5 m) did not allow transportation of the clasts and that the sediments were repeatedly in contact with the flowing ice, leading to abrasion. The upward improving sorting and stratification with weakly inclined beds toward the east and declining grain-size suggests deposition by stream flows, probably as shallow, braid bars within rapidly widening flow space.

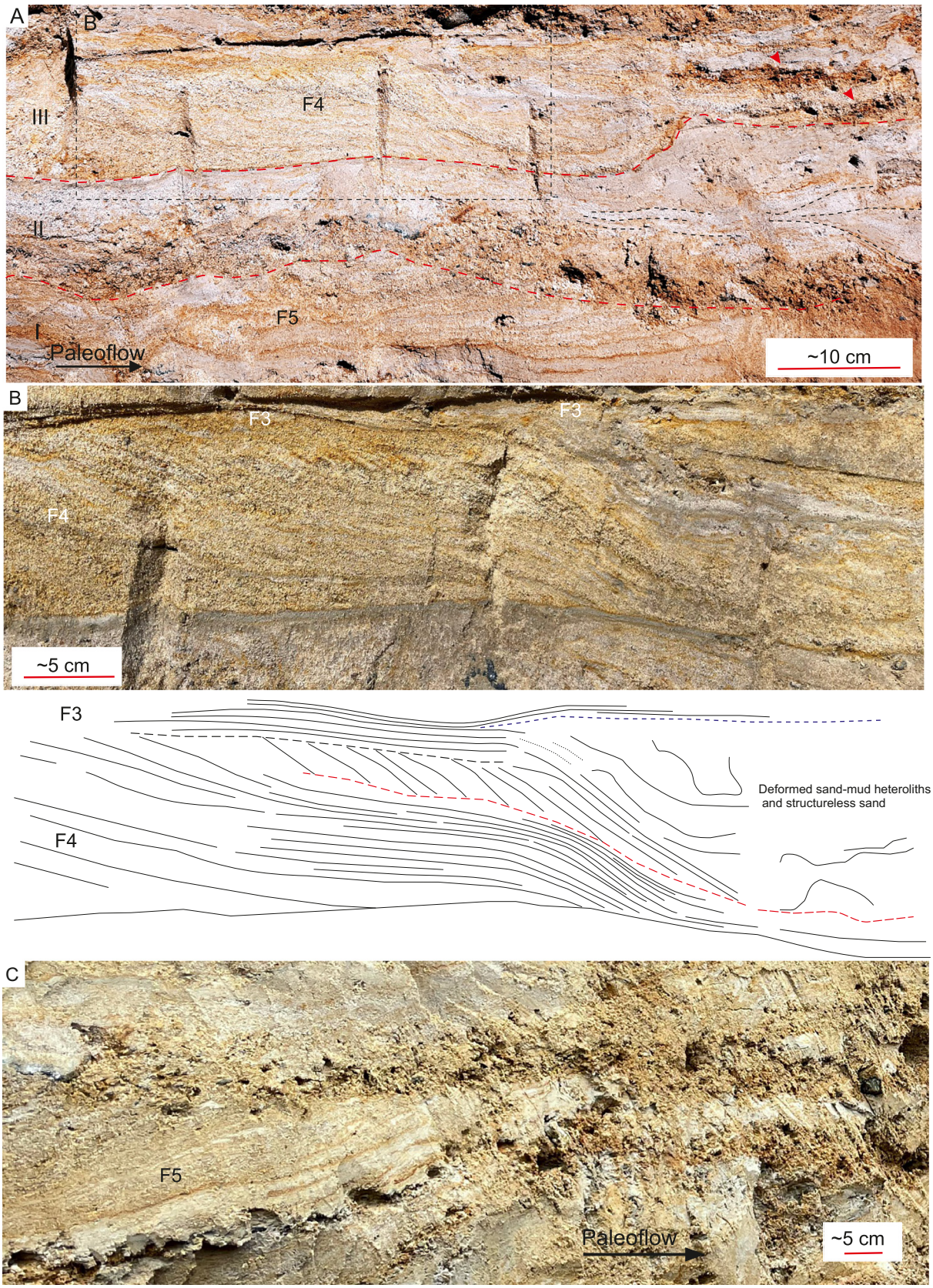

Fig. 6. A) A photo toward the north illustrating three stacked bedsets (I–III). See Table 1 for facies codes. Red stippled lines mark variably erosional bed boundaries. Black stippled lines highlight examples of undulating sand-beds. Red arrows point to minor granule-bearing scour fills. B) A close-up view and line drawing of sigmoidal cross-stratification. The deposits show two stacked cross-sets separated by an erosional surface (red line). The lower foreset deposits downlap onto the basal surface and display a transition between convex foreset beds and subhorizontal topset beds with rising and falling brink trajectories. The overlying smaller-scale cross-set shows straight foreset beds, which in turn are erosively overlain by sinusoidally-stratified topset beds (F3). C) A photo toward the north illustrating the solitary occurrence of upstream-oriented cross-stratification.

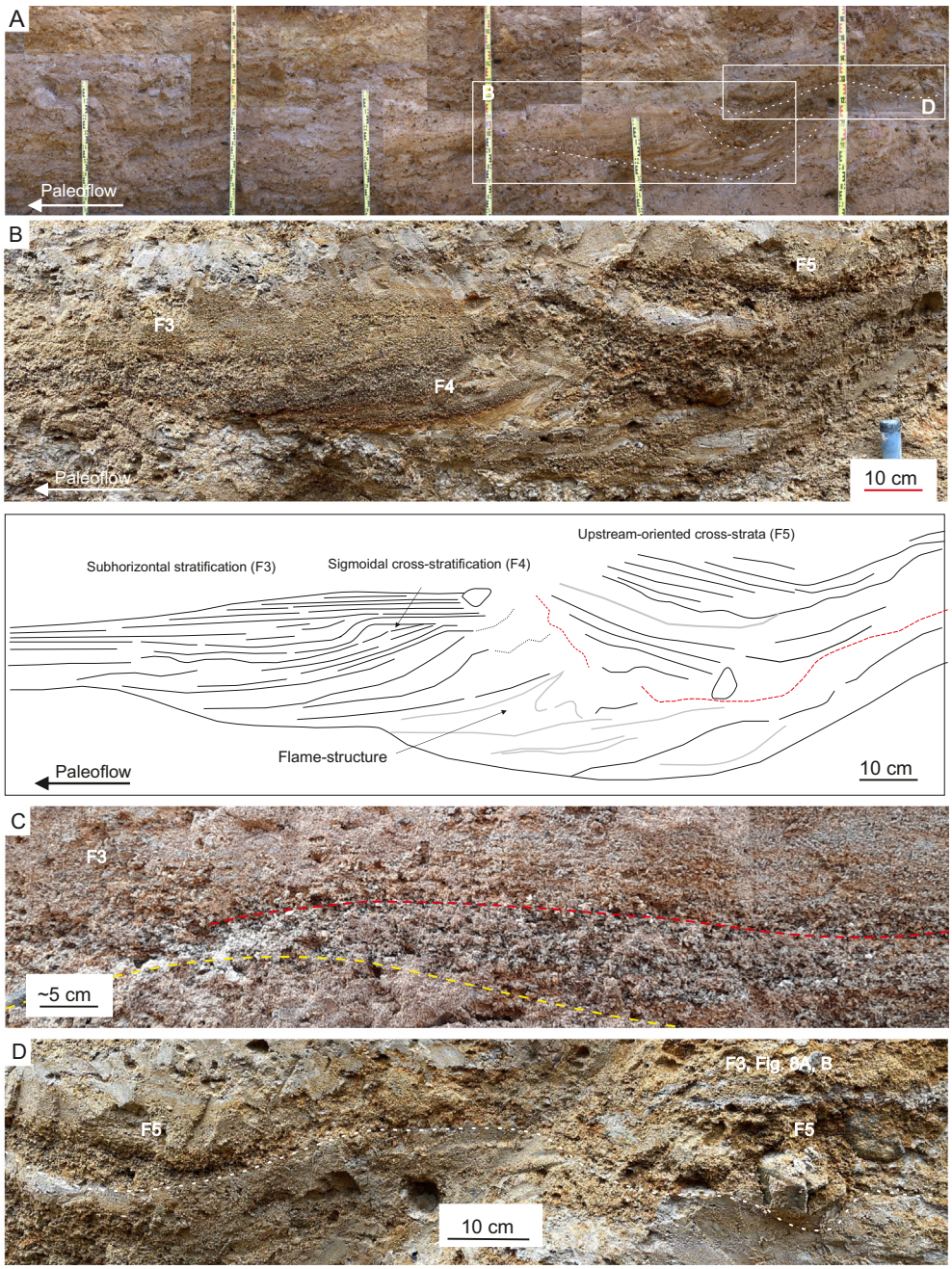

Fig. 7. A) A down-current inclined bed slope with various scours. See Fig. 2B for a wider photo panorama. B) Close-up view photo and line drawing of sigmoidal cross-stratification (F4) grading upward and downcurrent into subhorizontal stratification (F3). Upstream, the deposits are incised by a scour filled with backset cross-stratification (F5). The foreset of sigmoidal cross-stratification downlaps onto the basal scour surface and displays a transition between concave foreset beds and subhorizontal topset beds with a subhorizontal brink trajectory. C) Close-up view of subhorizontal stratification erosively overlying the bottom set of sigmoidal cross-stratification. The red stippled line marks the erosional contact, whereas the yellow stippled line indicates the basal scour surface. D) Close-up view of a scour fill with backset cross-stratification (F5) which can be traced laterally to a concave surface and further upstream into a chaotic, cobble-bearing scour fill. Fig. 8A–C shows the top of these scour fills and its overlying deposits.

Following the initial enlargement of the subglacial conduit (Phase 1 in Fig. 10), sand lenses, silt-drapes, sinusoidally stratified sand, and poorly-sorted gravel lenses were deposited in the proximal part of Unit C (Phase 2 in Fig. 10). In particular, silt laminae and beds are commonly draping ripple-scale bedforms or forming interbeds, indicating waning flows of the lower-flow regime and suspension fallout. No evidence for ice–sediment coupling is observed in Unit C. The largest out-sized clasts are cobbles, which suggests that the maximum flow depth was probably <25 cm.

Subsequently, between profiles P4 and P5 (Fig. 2), the increasing grain size, size of out-sized clasts (a-axis up to ~50 cm) and scale of cross-sets point to an increase in flow velocity and flow depths (Phase 3 in Fig. 10). The clasts are interpreted to be derived from the ice roof. The down-current inclined slope of almost 1 m height and 15 m length is in line with increasing water depth and development of an enlarged water-filled cavity or pond. The slope sediments are characterized by sinusoidal stratification, sigmoidal cross-stratification and scours with backsets or chaotic fill interpreted as upper-flow-regime deposits (discussed below). The final deposition resulted in murtoo head-bar development, the height of which indicates that the water depth approached 1 m.

Finally, the pond was rapidly closed by ice, as evidenced by the disappearance of sorted, stratified sediments and appearance of

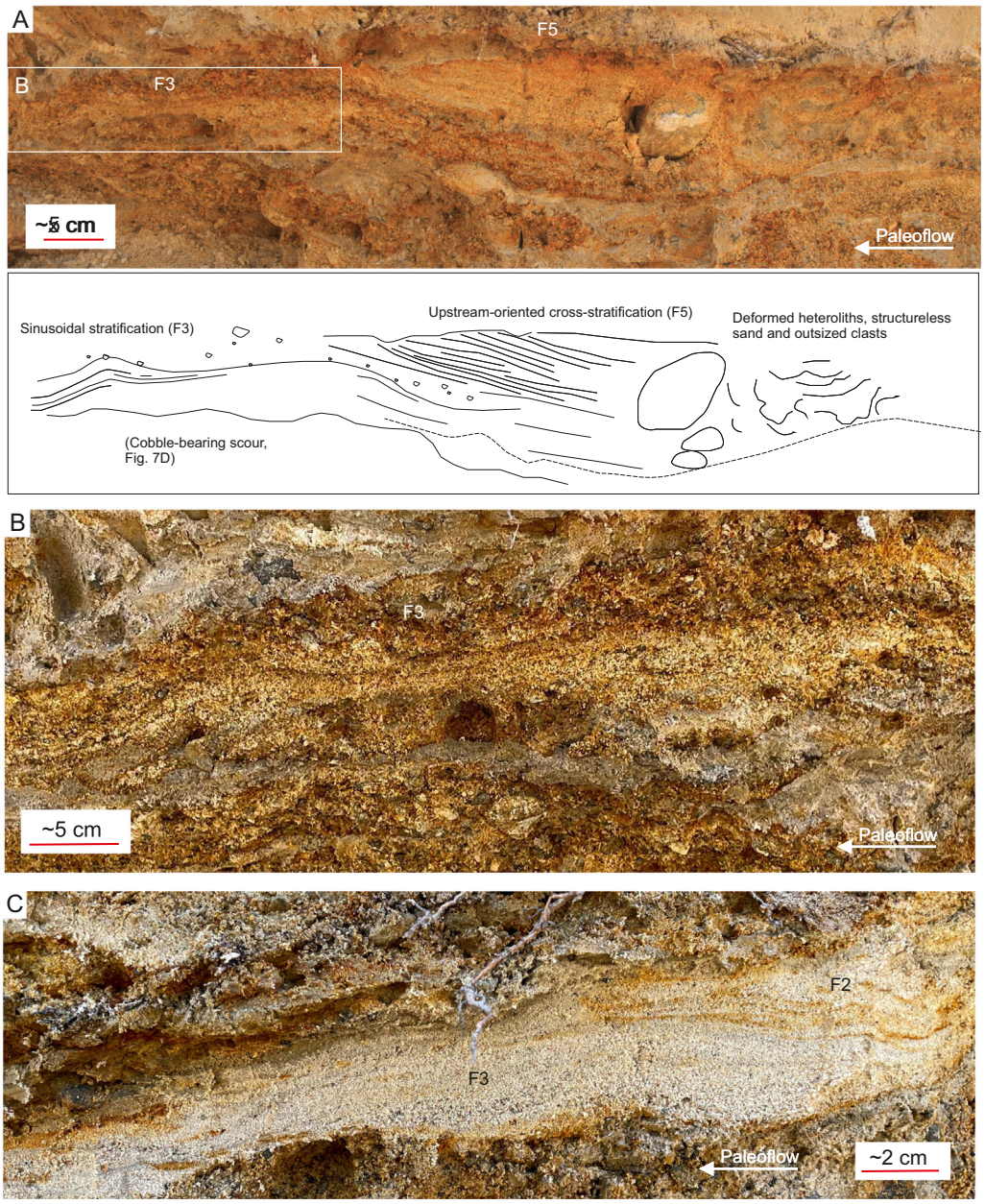

Fig. 8. A) A close-up view and line drawing of the top of a scour showing upstream-oriented cross-stratification. The upstream end of the scour contains deformed heteroliths and structureless sand with outsized clasts. The downstream end shows sinusoidal stratification. B) Close-up view of sinusoidal stratification shown in Fig. A. C) Sinusoidal stratification (F3) passing upward into ripple-scale upcurrent climbing bedform (F2).

compacted diamicton of Unit D (Phase 4 in Fig. 10). The ice–sediment coupling was local and closed only the broadened central part of the murtoo. Meltwater-flow processes continued along the sides of the murtoo (Unit E), being forced to pass the closed space and to flow obliquely toward the tip; this process potentially initiated the triangular development characteristic for murtoos (Peterson Becher and Johnson, 2021). Thus, the ice–sediment coupling coincided with further intensifying and increasingly erosional channelized glaciofluvial flow as indicated by boulder-rich proto-channel fills (Units E and F). The meltwater flow velocities finally dropped abruptly as evidenced by the development of clay plugs in the marginal channels of the murtoo (Unit F).

The deposits of Units C–E thus reflect an overall increase in meltwater delivery until its abrupt decay, which could be explained by a melt season or autogenic changes within the meltwater system. In previous works, murtoos have been interpreted to develop within a single melt season during deglaciation on top of the broad and low, arched deposits of the core (Mäkinen et al., 2023). Unit D is interpreted to represent localized ice–bed coupling caused by decreasing water pressure, as the subglacial drainage system became wider and better connected. The subsequent Units E and F (Figs. 2, 4A, B) reflect further increasing meltwater discharge and flow velocities, until its abrupt decay and abandonment.

4.2. Formation of upper-flow regime bedforms in a water-filled subglacial pond/cavity

As mentioned above, the deposition of Sub-unit C2 was related to a phase of cavity enlargement and pond formation by an increase in meltwater discharge (Phase 3 in Fig. 10). Characteristics are sandy deposits with upper-flow regime bedforms (Fig. 11). Upper-flow regime bedforms commonly form in subaerial open channel flows, where the

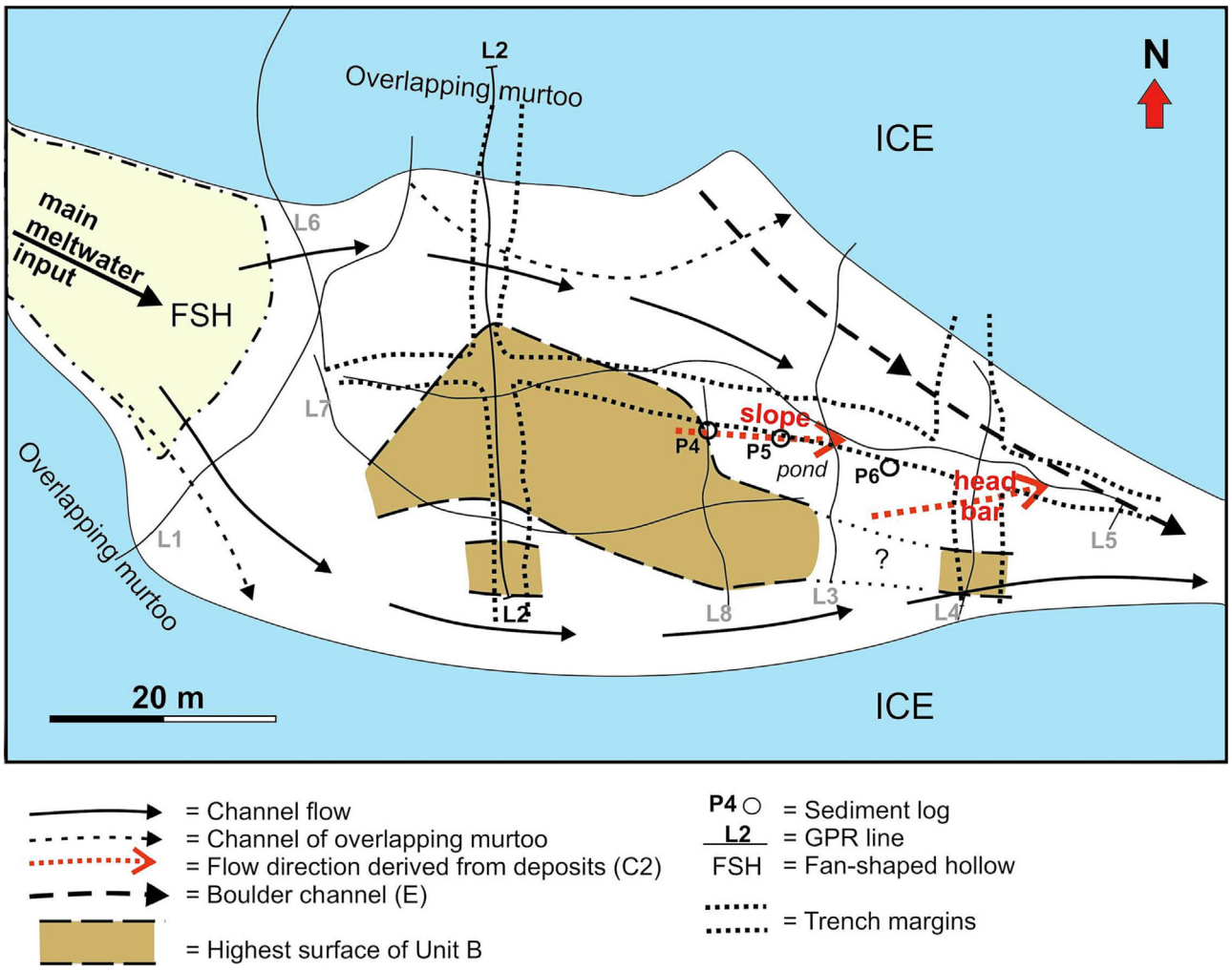

Fig. 9. A sketch illustrating the depositional environment of the murtoo. The highest surface area of Unit B is based on the GPR interpretation and trench observations. Note the position of the slope and murtoo head bar along the longitudinal trench 1 within a subglacial pond. The maximum depth of the pond was c. 1 m. See Fig. 3 for the interpretation of GPR profile L2 along the proximal cross-section.

upper boundary of the flow is the air–water interface, in density flows where the upper boundary of the flow is in contact with ambient water or at internal density boundaries within stratified flows (e.g., Cartigny et al., 2014; Postma and Cartigny, 2014; Fedele et al., 2016; Lang et al., 2017a, 2021b). Under subglacial pipe-flow conditions, the formation of supercritical flow conditions is suppressed (Banerjee and McDonald, 1975; Cartigny et al., 2014; Lang et al., 2021b), because there is no freely deformable flow surface (e.g., Cartigny et al., 2014). Therefore, supercritical flow conditions are unlikely in inefficient or semi-efficient distributed drainage systems, where only a centimeter- to decimeter-scale space exists between the ice and the bed (Banerjee and McDonald, 1975). However, previous work has demonstrated that UFR-bedforms may form in larger subglacial channels in efficient drainage systems under non-full pipe conditions (e.g., Brennand, 1994; Fiore et al., 2002; Burke et al., 2008, 2010; Lee et al., 2015) or in subglacial lakes, where supercritical density flows may develop on the slope. For example, McCabe and ÓCofaigh (1994) documented sinusoidally stratified sand beds, although they did not recognize these bedforms as antidune deposits.

The observed supercritical bedforms in Sub-unit C2 were most likely deposited by density flows on the slope of a water-filled subglacial pond/cavity (Fig. 11). Tank experiments and field data show that supercritical density flows may develop on the lee slope of mouth bars <1 m high (e.g., Lang et al., 2021a; Winsemann et al., 2021). The observed UFR-bedforms are generally small with decimeter-scale wavelengths and are comparable to bedforms described from various (glacio)lacustrine and marine deltas and fans (e.g., Lang and Winsemann, 2013; Lang et al., 2017a, 2017b, 2021b; Winsemann et al., 2018, 2021; Tan and Plink-Björklund, 2021). Sinusoidally stratified sand and ripple-scale climbing bedforms have also been described from subglacial ponds in Sweden and attributed to folding (Remmert et al., 2022). However, the deposits of this case study are not tectonically deformed and show only local soft-sediment deformation that is restricted to specific, mostly silt-rich beds. The studied sinusoidally stratified and ripple-scale climbing bedforms are closely associated with other UFR bedforms such as scours with backsets and sigmoidal cross-stratification, suggesting that the observed features are primary sedimentary structures.

The scoured, irregular slope topography may have formed by net-erosional cyclic steps during a major meltwater drainage event (cf. Fildani et al., 2006; Spinewine et al., 2009; Lang and Winsemann, 2013). These scours partly display progradational sandy infills, which resemble humpback dunes and laterally pass into antidune deposits. Laterally offset-stacked scour fills with deformed sediments and backsets represent the hydraulic jump zone of upstream migrating cyclic steps (e.g., Postma and Cartigny, 2014; Lang et al., 2017a, 2017b, 2021b; Winsemann et al., 2018; Slootman and Cartigny, 2020), which probably formed during successive flood events. Complex infills with prominent grain size breaks, mud-drapes and erosional surfaces point

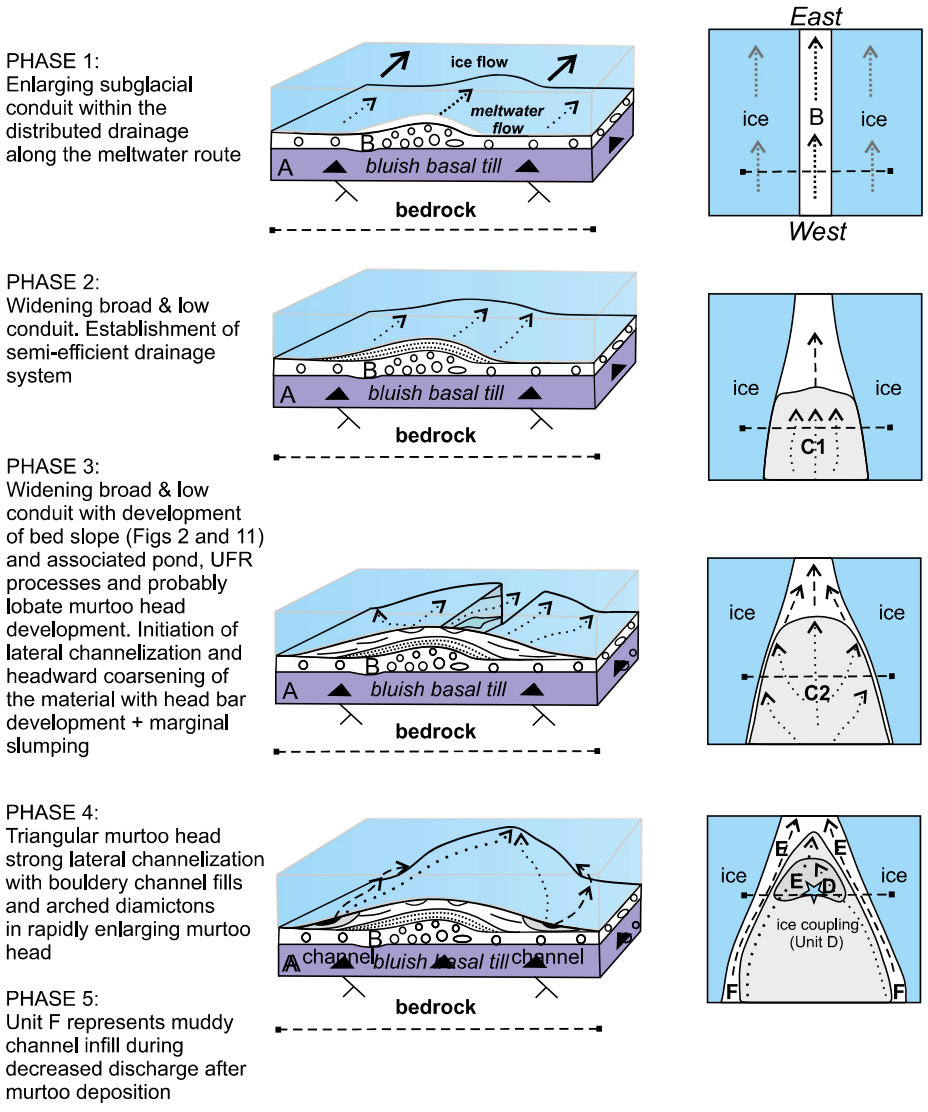

Fig. 10. Depositional phases of the murtoo. At right a schematic in-plan view illustrates the murtoo development superimposed on the subglacial meltwater route deposits (Unit B). The successive events reflect an initial increase in subglacial meltwater flow (Unit C), localized ice–bed coupling (Unit D), the erosion of the murtoo head during the peak flow (Unit E), and eventually to development of marginal channel deposits (Unit F) during the diminishing meltwater flow. Phase 3 (Unit C) represents the filling of the subglacial pond with maximum depth of ca. 1 m and the related deposition of the upper-flow-regime bedforms. The dashed lines across the in-plan views indicate the position of the drawing at left.

to pulsating flows. These deposits typically pass laterally and vertically into antidune deposits. This lateral and vertical association of chutes-and-pools, cyclic step, and antidune deposits is commonly observed in the geologic record, suggesting a relation to the spatio-temporal evolution of the formative flow and the re-establishment of supercritical flow conditions on the stoss-sides of cyclic steps (e.g., Lang and Winsemann, 2013; Cartigny et al., 2014; Postma et al., 2014; Zhong et al., 2015; Lang et al., 2017a, 2017b, 2021b; Winsemann et al., 2018; Slootman and Cartigny, 2020). The final coarse-grained murtoo head-bar development, characterized by planar-cross stratified gravel and pebbly sand, indicates avalanche processes that were controlled by grain size (cf., Winsemann et al., 2021). The phase of cavity enlargement (Phase 3 in Fig. 10) ultimately led to a decrease in water pressure and creep closure by ice.

5. Conclusions

Our study provides an insight into the early evolution of a murtoo landform as well as the temporal and spatial transition from a subglacial inefficient drainage toward an efficient drainage system. The results demonstrate that the core of the murtoo is depositional and that it was formed by meltwater. The deposition of the studied interval (Unit C) took place during intensifying meltwater delivery. The subsequent flow was powerful and characteristically erosional and channelized until the abrupt abandonment and end of murtoo sedimentation (Units E and F).

Unit C comprises 7 facies types, which are interpreted to represent various lower- and upper-flow regime bedforms. The initial deposition in the proximal part of the murtoo was dominated by fine-grained deposits of the lower-flow regime in a shallow semi-efficient drainage system. The subsequent sedimentation reflects an increase in flow velocity and water depth and was characterized by the development of a slope and an associated enlarged water-filled cavity/pond. The slope sediments show typical upper-flow-regime bedforms such as sinusoidal stratification, sigmoidal cross-stratification, scours with backsets or chaotic fill, interpreted as deposits of antidunes, humpback dunes, chutes-and-pools and cyclic steps. The increased water depth led to a rapid drop in water pressure and localized, intra-melt season ice–bed coupling.

The presence of UFR bedforms indicates that, despite the overall shallow space and water depth, the causative flows reached non-full

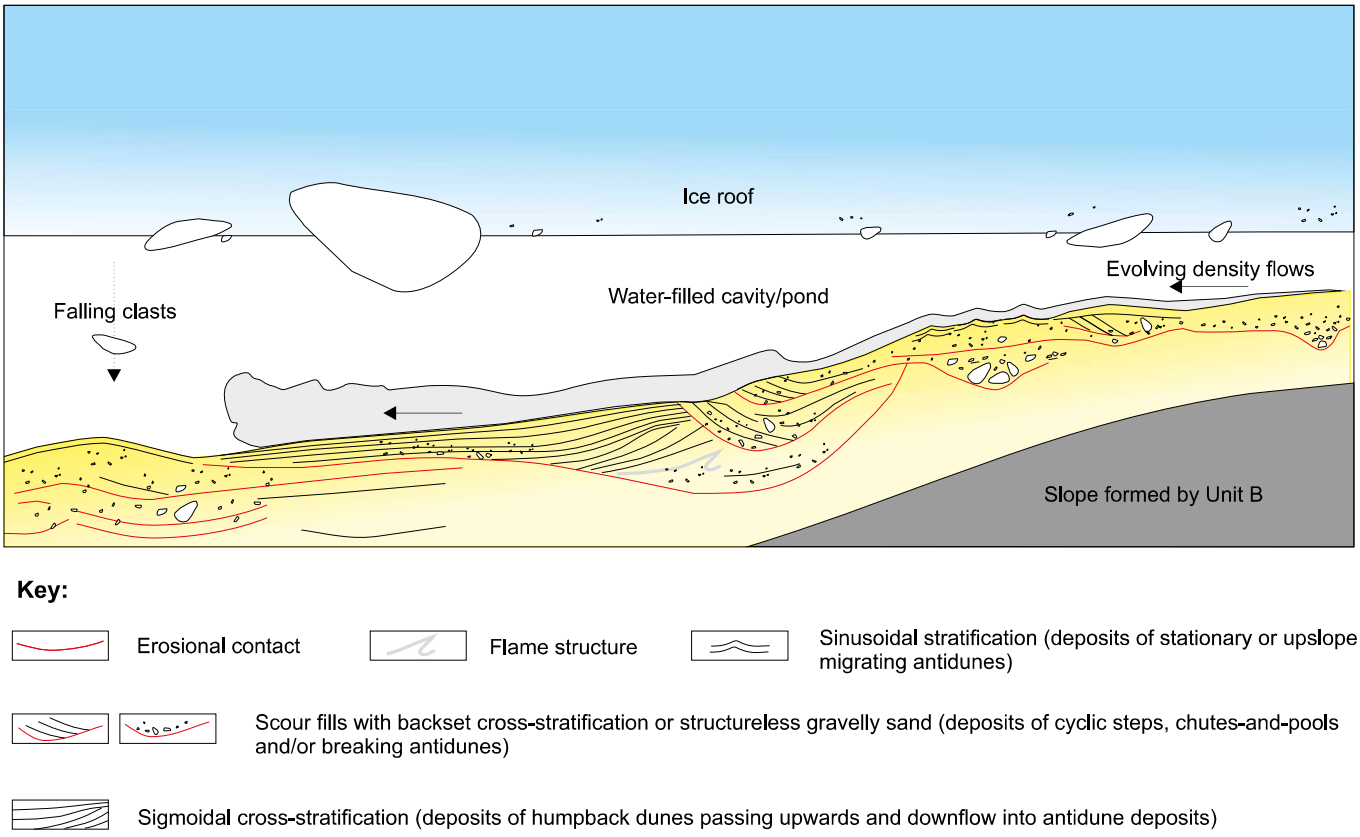

Fig. 11. A schematic illustration showing characteristic supercritical flow deposits on the slope of the enlarged cavity/pond.

pipe flow conditions, particularly in the pond. Most likely, the supercritical deposits were deposited by density flows. The final coarse-grained murtoo head-bar development, characterized by planar-cross stratified gravel and pebbly sand, indicates avalanche processes that were controlled by grain size.

In concert, the results indicate that murtoo deposition begins with a rapid increase in meltwater discharge into an evolving flow space and is followed by flow channelization along the murtoo margins. Thus, murtoos form an important element for the modeling of subglacial hydrology and related prediction of glacial dynamic response to increased meltwater delivery. The combination of murtoo morphology and the growing understanding of internal structures and depositional evolution will enable future investigations into whether there is genetic diversity in murtoo landforms or whether their formation can be explained by a single formation model.

Data availability

Data will be made available on request.

Declaration of competing interest

The authors declare that they have no known competing financial interests or personal relationships that could have appeared to influence the work reported in this paper.

Acknowledgements

This work is part of the RewarD project (MUST consortium), funded by the Academy of Finland (grant numbers 322243/Joni Mäkinen, University of Turku and 322252/Antti Ojala, University of Turku). We are grateful for Giorgio Basilici and an anonymous reviewer for constructive and insightful comments that improved paper.

References

Ahokangas, E., Ojala, A.E., Tuunainen, A., Valkama, M., Palmu, J.P., Kajuutti, K., Mäkinen, J., 2021. The distribution of glacial meltwater routes and associated murtoo fields in Finland. Geomorphology 389, 107854.

Alexander, J., Bridge, J.S., Cheel, R.J., Leclair, S.F., 2001. Bedforms and associated sedimentary structures formed under supercritical water flows over aggrading sand beds. Sedimentology 48, 133–152.

Allen, J.R.L., 1982. Sedimentary structures: their character and physical basis. Developments in Sedimentology 30, 1–663.

Andrews, L.C., Catania, G.A., Hoffman, M.J., Gulley, J.D., Lüthi, M.P., Ryser, C., Neumann, T. A., 2014. Direct observations of evolving subglacial drainage beneath the Greenland Ice Sheet. Nature 514, 80–83.

Banerjee, I., McDonald, B.C., 1975. Nature of esker sedimentation. In: Jopling, A.V., McDonald, B.C. (Eds.), Glaciofluvial and Glaciolacustrine Sedimentation. SEPM Special Publicationsvol. 23, pp. 304–320.

Best, J., Bridge, J., 1992. The morphology and dynamics of low amplitude bedwaves upon upper stage plane beds and the preservation of planar laminae. Sedimentology 39, 737–752.

Boulton, G.S., Dongelmans, P., Punkari, M., Broadgate, M., 2001. Palaeoglaciology of an ice sheet through a glacial cycle: the European ice sheet through the Weichselian. Quaternary Science Reviews 20, 591–625.

Brennand, T.A., 1994. Macroforms, large bedforms and rhythmic sedimentary sequences in subglacial eskers, south-central Ontario: implications for esker genesis and meltwater regime. Sedimentary Geology 91, 9–55.

Burke, M.J., Woodward, J., Russell, A.J., Fleisher, P.J., Bailey, P.K., 2008. Controls on the sedimentary architecture of a single event englacial esker: Skeiðarárjökull, Iceland. Quaternary Science Reviews 27, 1829–1847.

Burke, M.J., Woodward, J., Russell, A.J., Fleisher, P.J., Bailey, P.K., 2010. The sedimentary architecture of outburst flood eskers: a comparison of ground-penetrating radar data from Bering Glacier, Alaska and Skeiðarárjökull, Iceland. GSA Bulletin 122, 1637–1645.

Cartigny, M.J.B., Ventra, D., Postma, G., Den Berg, J.H., 2014. Morphodynamics and sedimentary structures of bedforms under supercritical-flow conditions: new insights from flume experiments. Sedimentology 61, 712–748.

de Cala, I., Ohata, K., Dorrell, R., Naruse, H., Patacci, M., Amy, L.A., Simmons, S., McLelland, S.J., McCaffrey, W.D., 2020. Relating the flow processes and bedforms of steady-state and waning density currents. Frontiers in Earth Science 8.

Dewald, N., Livingstone, S.J., Clark, C.D., 2022. Subglacial meltwater routes of the Fennoscandian Ice Sheet. Journal of Maps https://doi.org/10.1080/17445647.2022.2071648.

Dietrich, P., Ghienne, J.-F., Normandeau, A., Lajeunesse, P., 2016. Upslope-migrating bedforms in a proglacial sandur delta: cyclic steps from river-derived underflows? Journal of Sedimentary Research 86, 113–123.
Fedele, J.J., Hoyal, D.C., Barnaal, Z., Tulenko, J., Awalt, S., 2016. Bedforms created by gravity flows. In: Budd, D., Hajek, E., Purkis, S. (Eds.), Autogenic Dynamics In Sedimentary Systems. SEPM Special Publicationsvol. 106, pp. 95–121.
Fielding, C.R., 2006. Upper flow regime sheets, lenses and scour fills: extending the range of architectural elements for fluvial sediment bodies. Sedimentary Geology 190, 227–240.
Fildani, A., Normark, W.R., Kostic, S., Parker, G., 2006. Channel formation by flow stripping: large-scale scour features along the Monterey East Channel and their relation to sediment waves. Sedimentology 53, 1265–1287.
Ghienne, J.-F., Normandeau, A., Dietrich, P., Bouysson, M., Lajeunesse, P., Schuster, M., 2021. The depositional signature of cyclic steps: a late Quaternary analogue compared to modern active delta slopes. Sedimentology 68, 1502–1538. https://doi.org/10.1111/sed.12806.
Girard, F., Ghienne, J., Rubino, J.L., 2012. Occurrence of hyperpyncal flows and hybrid event beds related to glacial outburst events in a Late Ordovician proglacial delta (Murzuq Basin, SW Libya). Journal of Sedimentary Research 82, 688–708.
Hand, B.M., 1974. Supercritical flow in density currents. Journal of Sedimentary Research 44, 637–648.
Hart, J.K., Young, D.S., Baurley, N.R., et al., 2022. The seasonal evolution of subglacial drainage pathways beneath a soft-bedded glacier. Communications Earth and Environment 3, 152. https://doi.org/10.1038/s43247-022-00484-9.
Hirst, J.P.P., Benbakir, A., Payne, D.F., Westlake, I.R., 2002. Tunnel valleys and density flow processes in the Upper Ordovician glacial succession, Illizi Basin, Algeria: influence on reservoir quality. Journal of Petroleum Geology 25, 297–324.
Hodgson, D.A., Roberts, S.J., Bentley, M.J., Carmichael, E.L., Smith, J.A., Verleyen, E., Vyverman, W., Geissler, P., Leng, M.J., Sanderson, D.C., 2009. Exploring former subglacial Hodgson Lake, Antarctica. Paper II: palaeolimnology. Quaternary Science Reviews 28, 2310–2325.
Hooke, R.L., 2019. Principles of Glacier Mechanics. Cambridge University Press.
Kennedy, J.F., 1963. The mechanics of dunes and antidunes in erodible-bed channels. Journal of Fluid Mechanics 16, 521–544. https://doi.org/10.1017/S0022112063000975.
Lang, J., Winsemann, J., 2013. Lateral and vertical facies relationships of bedforms deposited by aggrading supercritical flows: from cyclic steps to humpback dunes. Sedimentary Geology 296, 36–54.
Lang, J., Brandes, C., Winsemann, J., 2017a. Erosion and deposition by supercritical density flows during channel avulsion and backfilling: field examples from coarse-grained deepwater channel–levée complexes (Sandino Forearc Basin, southern Central America). Sedimentary Geology 349, 79–102.
Lang, J., Sievers, J., Loewer, M., Igel, J., Winsemann, J., 2017b. 3D architecture of cyclic-step and antidune deposits in glacigenic subaqueous fan and delta settings: integrating outcrop and ground-penetrating radar data. Sedimentary Geology 362, 83–100.
Lang, J., Fedele, J.J., Hoyal, D.C., 2021a. Three-dimensional submerged wall jets and their transition to density flows: morphodynamics and implications for the depositional record. Sedimentology 68, 1297–1327.
Lang, J., Le Heron, D.P., Van den Berg, J.H., Winsemann, J., 2021b. Bedforms and sedimentarystructures related to supercritical flows in glacigenic settings. Sedimentology 68, 1539–1579.
Lee, J.R., Wakefield, O.J., Phillips, E., Hughes, L., 2015. Sedimentary and structural evolution of a relict subglacial to subaerial drainage system and its hydrogeological implications: an example from Anglesey, north Wales, UK. Quaternary Science Reviews 109, 88–110.
Lesemann, J.-E., Alsop, G.I., Piotrowski, J.A., 2010. Incremental subglacial meltwater sediment deposition and deformation associated with repeated ice–bed decoupling: a case study from the Island of Funen, Denmark. Quaternary Science Reviews 23–24, 3212–3229.
Mäkinen, J., Kajuutti, K., Palmu, J.-P., Ojala, A., Ahokangas, E., 2017. Triangular-shaped landforms reveal subglacial drainage routes in SW Finland. Quaternary Science Reviews 164, 37–53.
Mäkinen, J., Kajuutti, K., Ojala, A., Ahokangas, E., Palmu, J.-P., 2019. Sedimentary characteristics of Finnish MURTOOs - triangular-shaped subglacial landforms produced during rapid retreat of continental ice sheets. Advances in Glacier Hydrology III Posters, C13C-1309. AGU Fall Meeting San Francisco CA, 9–13 December 2019.
Mäkinen, J., Kajuutti, K., Ojala, A.E.K., Ahokangas, E., Tuunainen, A., Valkama, M., et al., 2023. Genesis of subglacial triangular-shaped landforms (murtoos) formed by the Fennoscandian Ice Sheet. Earth Surface Processes and Landforms, 1–26 https://doi.org/10.1002/esp.5606.
McCabe, A.M., ÓCofaigh, C., 1994. Sedimentation in a subglacial lake, Enniskerry, eastern Ireland. Sedimentary Geology 91, 57–95.
Munro-Stasiuk, M.J., 2003. Subglacial Lake McGregor, south-central Alberta, Canada. Sedimentary Geology 160, 325–350.
Nienow, P.W., Sole, A.J., Slater, D.A., Cowton, T.R., 2017. Recent advances in our understanding of the role of meltwater in the Greenland Ice Sheet system. Current Climate Change Reports 3, 330–344. https://doi.org/10.1007/s40641-017-0083-9.
Ojala, A.E.K., Palmu, J.-P., Åberg, A., Åberg, S., Virkki, H., 2013. Development of an ancient shoreline database to reconstruct the Litorina Sea maximum extension and the highest shoreline of the Baltic Sea basin in Finland. Bulletin of the Geological Society of Finland 85, 127–144.
Ojala, A.E.K., Peterson, G., Mäkinen, J., Johnson, M., Kajuutti, K., Ahokangas, E., Palmu, J.-P., Ohrling, C., 2019. Ice sheet scale distribution of unique triangular-shaped hummocks (murtoos)—a subglacial landform produced during rapid retreat of the Scandinavian Ice Sheet. Annals of Glaciology 60, 115–126.
Ojala, A.E., Mäkinen, J., Kajuutti, K., Ahokangas, E., Palmu, J.P., 2022. Subglacial evolution from distributed to channelized drainage: evidence from the Lake Murtoo area in SW Finland. Earth Surface Processes and Landforms 47, 2877–2896.
Palmu, J.-P., Ojala, A.E.K., Virtasalo, J., Putkinen, N., Kohonen, J., Sarala, P., 2021. Classification system of superficial (Quaternary) geological units in Finland. Geological Survey of Finland, Bulletin 412, 115–169. https://doi.org/10.30440/bt412.
Paola, C., Wiele, S., Reinhart, M., 1989. Upper-regime parallel lamination as the result of turbulent sediment transport and low-amplitude bed forms. Sedimentology 36, 47–59.
Peterson Becher, G., Johnson, M.D., 2021. Sedimentology and internal structure of murtoos - V-shaped landforms indicative of a dynamic subglacial hydrological system. Geomorphology 380, 107644. https://doi.org/10.1016/j.geomorph.2021.107644.
Peterson, G., Johnson, M.D., 2017. Hummock corridors in the south-central sector of the Fennoscandian ice sheet, morphometry and pattern. Earth Surface Processes and Landforms 43, 919–929.
Postma, G., Cartigny, M.J.B., 2014. Supercritical and subcritical turbidity currents and their deposits—a synthesis. Geology 42, 987–990.
Postma, G., Kleverlaan, K., Cartigny, M.J.B., 2014. Recognition of cyclic steps in sandy and gravelly turbidite sequences, and consequences for the Bouma facies model. Sedimentology 61, 2268–2290.
Ravier, É., Lelandais, T., Vérité, J., Bourgeois, O., 2022. Variations in hydraulic efficiency of the subglacial drainage landsystem control surging and streaming regimes of outlet glaciers. Journal of Glaciology, 1–19 https://doi.org/10.1017/jog.2022.107.
Remmert, I., Johnson, M.D., Ström, O.J., Peternell, M., Becher, G.P., 2022. Seasonal subglacial ponding deposits in a thick till sequence, Dösebacka drumlin, southwest Sweden. Sedimentary Geology 440, 106241.
Russell, H.A.J., Arnott, R.W.C., Sharpe, D.R., 2003. Evidence for rapid sedimentation in a tunnel channel, Oak Ridges Moraine, southern Ontario, Canada. Sedimentary Geology 160, 33–55.
Russell, H.A.J., Sharpe, D.R., Bajk, A.F., 2007. Sedimentary signatures of the Waterloo Moraine, Ontario, Canada. In: Hambrey, M., Christoffersen, P., Glasser, N., Hubbard, B. (Eds.), Glacial Processes and Products. IAS Special Publicationsvol. 39, pp. 85–108.
Saunderson, H.C., Lockett, F.P.J., 1983. Flume experiments on bedforms and structures at the dune-plane bed transition. In: Collinson, J.D., Lewin, L. (Eds.), Modern and Ancient Fluvial Systems. IAS Special Publicationsvol. 6, pp. 49–58.
Schoof, C., 2010. Ice sheet acceleration driven by melt supply variability. Nature 468, 803–806.
Simkins, L.M., Greenwood, S.L., Winsborrow, M.C.M., Bjarnadóttir, L.R., Lepp, A.P., 2023. Advances in understanding subglacial meltwater drainage from past ice sheets. Annals of Glaciology, 1–5 https://doi.org/10.1017/aog.2023.16.
Slootman, A., Cartigny, M.J., 2020. Cyclic steps: review and aggradation-based classification. Earth-Science Reviews 201, 102949.
Slootman, A., Vellinga, A.J., Moscariello, A., Cartigny, M.J.B., 2021. The depositional signature of high-aggradation chute-and-pool bedforms: the build-and-fill structure. Sedimentology 68, 1640–1673.
Spinewine, B., Sequeiros, O.E., Garcia, M.H., Beaubouef, R.T., Sun, T., Savoye, B., Parker, G., 2009. Experiments on wedge-shaped deep sea sedimentary deposits in minibasins and/or on channel levees emplaced by turbidity currents. Part II. Morphodynamics of the wedge and of the associated bedforms. Journal of Sedimentary Research 79, 608–628.
Stroeven, A.P., Hättestrand, C., Kleman, J., Heyman, J., Fabel, D., Fredin, O., Goodfellow, B. W., Harbor, J.M., Jansen, J.D., Olsen, L., Caffee, M.W., Fink, D., Lundqvist, J., Rosqvist, G.C., Strömberg, B., Jansson, K.N., 2016. Deglaciation of Fennoscandia. Quaternary Science Reviews 147, 91–121. https://doi.org/10.1016/j. quascirev.2015.09.016.
Tan, C., Plink-Björklund, P., 2021. Morphodynamics of supercritical flow in a linked river and delta system, Daihai Lake, Northern China. Sedimentology 68, 1606–1639.
Werder, M.A., Hewitt, I.J., Schoof, C.G., Flowers, G.E., 2013. Modeling channelized and distributed subglacial drainage in two dimensions. JGR: Earth Surface 118, 2140–2158. https://doi.org/10.1002/jgrf.20146.
Winsemann, J., Hornung, J.J., Meinsen, J., Asprion, U., Polom, U., Brandes, C., Bußmann, M., Weber, C., 2009. Anatomy of a subaqueous ice-contact fan and delta complex, Middle Pleistocene, NW Germany. Sedimentology 56, 1041–1076.
Winsemann, J., Lang, J., Polom, U., Loewer, M., Igel, J., Pollok, L., Brandes, C., 2018. Ice-marginal forced regressive deltas in glacial lake basins: geomorphology, facies variability and large-scale depositional architecture. Boreas 47, 973–1002.
Winsemann, J., Lang, J., Fedele, J.J., Zavala, C., Hoyal, D.C., 2021. Re-examining models of shallow-water deltas: insights from tank experiments and field examples. Sedimentary Geology 421, 105962.
Zhong, G., Cartigny, M.J.B., Kuang, Z., Wang, L., 2015. Cyclic steps along the South Taiwan Shoal and West Penghu submarine canyons on the northeastern continental slope of the South China Sea. GSA Bulletin 127, 804–824.